Biomolecular NMR Assignments (2024) 18:71–78
https://doi.org/10.1007/s12104-024-10170-w

ARTICLE

^{1}H, ^{13}C, and ^{15}N resonance assignments and solution structure of the N-terminal divergent calponin homology (NN-CH) domain of human intraflagellar transport protein 54

Kanako Kuwasako[1,2,3] · Weirong Dang[1] · Fahu He[1] · Mari Takahashi[1,2] · Kengo Tsuda[1] · Takashi Nagata[1,4] · Akiko Tanaka[1] · Naohiro Kobayashi[1,5] · Takanori Kigawa[1,2] · Peter Güntert[6,7,8,9] · Mikako Shirouzu[1,2] · Shigeyuki Yokoyama[1,10,11] · Yutaka Muto[1,2,3]

Received: 28 November 2023 / Accepted: 13 March 2024 / Published online: 29 March 2024

Abstract

The intraflagellar transport (IFT) machinery plays a crucial role in the bidirectional trafficking of components necessary for ciliary signaling, such as the Hedgehog, Wnt/PCR, and cAMP/PKA systems. Defects in some components of the IFT machinery cause dysfunction, leading to a wide range of human diseases and developmental disorders termed ciliopathies, such as nephronophthisis. The IFT machinery comprises three sub-complexes: BBsome, IFT-A, and IFT-B. The IFT protein 54 (IFT54) is an important component of the IFT-B sub-complex. In anterograde movement, IFT54 binds to active kinesin-II, walking along the cilia microtubule axoneme and carrying the dynein-2 complex in an inactive state, which works for retrograde movement. Several mutations in IFT54 are known to cause Senior-Loken syndrome, a ciliopathy. IFT54 possesses a divergent Calponin Homology (CH) domain termed as NN-CH domain at its N-terminus. However, several aspects of the function of the NN-CH domain of IFT54 are still obscure. Here, we report the ^{1}H, ^{15}N, and ^{13}C resonance assignments of the NN-CH domain of human IFT54 and its solution structure. The NN-CH domain of human IFT54 adopts essentially the α1–α2–α3–α4–α5 topology as that of mouse IFT54, whose structure was determined by X-ray crystallographic study. The structural information and assignments obtained in this study shed light on the molecular function of the NN-CH domain in IFT54.

Keywords Intraflagellar transport (IFT) machinery · NN-CH domain · IFT54 · IFT-B2 · Ciliopathy

Kanako Kuwasako and Weirong Dang contributed equally to this work.

✉ Shigeyuki Yokoyama
yokoyama@riken.jp

✉ Yutaka Muto
ymuto@musashino-u.ac.jp

[1] RIKEN, Systems and Structural Biology Center, 1-7-22 Suehiro-cho, Tsurumi, Yokohama 230-0045, Japan

[2] RIKEN Center for Biosystems Dynamics Research, 1-7-22 Suehiro-cho, Tsurumi-ku, Yokohama 230- 0045, Japan

[3] Faculty of Pharmacy and Research Institute of Pharmaceutical Sciences, Musashino University, Tokyo 202-8585, Japan

[4] Institute of Advanced Energy, Graduate School of Energy Science, Kyoto University, Gokasho, Kyoto, Uji 611-0011, Japan

[5] RIKEN Yokohama NMR Facility, 1-7-22 Suehiro-cho, Tsurumi-ku, Yokohama 230-0045, Japan

[6] Tatsuo Miyazawa Memorial Program, RIKEN Genomic Sciences Center, Yokohama 230-0045, Japan

[7] Institute of Biophysical Chemistry, Goethe-University Frankfurt am Main, Max-von-Laue-Str. 9, Frankfurt am Main 60438, Germany

[8] Institute of Molecular Physical Science, ETH Zurich, Vladimir-Prelog-Weg 2, Zurich 8093, Switzerland

[9] Department of Chemistry, Tokyo Metropolitan University, 1-1 Minami-Ohsawa, Hachioji, Tokyo 192- 0397, Japan

[10] RIKEN Structural Biology Laboratory, 1-7-22 Suehiro-cho, Tsurumi-ku, Yokohama 230-0045, Japan

[11] RIKEN Cluster for Science, Technology and Innovation Hub, 1-7-22 Suehiro-cho, Tsurumi, Yokohama, Yokohama 230-0045, Japan

Biological context

In almost all vertebrate cells, cilia are microtubule-based organelles that protrude from the cell membrane. They sense outside's flow-changes and mediate several cell-signaling pathways essential for development and tissue homeostasis, such as the Hedgehog, Wnt, and cAMP/PKA signaling systems (Huangfu et al. 2003; Ishikawa et al. 2011; Richey et al. 2012; Braun et al. 2017; Wheway et al. 2018). At the base of the cilia, the intraflagellar transport (IFT) machinery plays a crucial role in the selection of components necessary for cilia assembly and ciliary signaling. The IFT machinery transports these components to the ciliary tip and successively mediates their return to the cell body in the ciliary bedrock (Kozminski et al. 1995; Wingfield et al. 2017).

The IFT machinery comprises three protein complexes: BBsome, IFT-A, and IFT-B (Cole et al. 1998; Piperno et al. 1998; Rosenbaum et al. 2002; Nachury et al. 2007; Taschner et al. 2016a, b; Ishikawa et al. 2017; Klena et al. 2022). BBsomes function as adaptors for the GPCR responsible for the above-mentioned signaling systems. During anterograde movement, the IFT-B complex binds to active kinesin-II, which walks on the cilia microtubule axoneme to the top of the cilia, carrying the inactive dynein-2 complex. During retrograde movement, dynein-2 complexes are bound to the IFT-A complex and are activated to walk on the cilia microtubule axoneme back to the bottom of the cilia (Hiyamizu et al. 2023a, b; Jordan et al. 2018; Funabashi et al. 2018). The IFT-A and IFT-B complexes are composed of six and 16 protein components, respectively. Furthermore, the IFT-B complex can be subdivided into the IFT-B1 (core 10 components) and IFT-B2 (peripheral 6 components) sub-complexes (Taschner et al. 2016a, b; Lacey et al. 2023; Petriman et al. 2022), which contain binding sites for ciliary cargo and inactive dynein-2 complexes, respectively (Hiyamizu et al. 2023a, b; Zhu et al. 2021). Defects in the components of the IFT machinery are known to cause aberrant cilia structure, leading to a wide range of human diseases and developmental disorders termed ciliopathies, such as nephronophthisis (Salomon et al. 2009; Tobin et al. 2009; Wolf et al. 2015).

IFT54, which is also termed MIP-T3 (microtubule-interacting protein associated with TRAF3) or TRAF3IP1 (TNF Receptor-Associated Factor 3 Interacting Protein 1), is a component of the IFT-B2 sub-complex (Ling et al. 2000). It is also known that several mutations in IFT54 cause Senior-Loken syndrome, which is a ciliopathy (Berbari et al. 2011). IFT54 is composed of 625 amino acid residues and possesses two well-established protein domains: the divergent calponin homology (NN-CH domain), spanning residues 1–135 at its N-terminus (deduced from the primary sequence alignment comparison to the NN-CH domain of Chlamydomonas (Zhu et al. 2021) and the coiled-coil domain spanning residues 525–625 at its C-terminus (Ling et al. 2000). The coiled-coil domain of IFT54 mediates its interaction with the other components of IFT-B2 and IFT20 (Katoh et al. 2016; Zhu et al. 2017). The region between the two established domains contains peptide segments that interact with the driving molecules, kinesin-II and the dynein-2 complex, during anterograde movement (Zhu et al. 2021). The regions spanning residues 261–275 and that spanning residues 342–356 of Chlamydomonas IFT54 directly interact with D1bLIC of the inactive dynein-2 complex and active kinesin-II, respectively (Hiyamizu et al. 2023a, b). These above-mentioned regions of IFT54 are critical for ciliary function.

However, some aspects of the function of the NN-CH domain of IFT54 remain to be elucidated. The calponin homology (CH) domain, which was first identified in calponin, is a common peptide module of approximately 100 residues, with a common tryptophan (W) residue and the consensus motif DGXXLXXL (Yin et al. 2020) (Supplementary Fig. 1). The protein fold was identified as the actin-binding module. Successively, it has been revealed that the CH domain can bind to another cytoskeletal protein, or tubulin, exemplified by the CH domain of the end-binding protein 1 (EB1) (Maurer et al. 2012). The tubulin-binding modes of the canonical CH domains of yeast Mal3 and EB3 (a paralog of EB1) proteins were elucidated by cryo-EM studies (Maurer et al. 2012; Zhang et al. 2015). Thus, the CH domain is considered to be a protein module that interacts with actin and/or tubulin to regulate cytoskeletal dynamics and signaling.

Among the subcomponents of the IFT machinery, a distinct CH domain was not identified, which was characterized by the above-mentioned conserved Trp residue and a common amino acid sequence (Supplementary Fig. 1). However, profile-to-profile sequence analysis revealed that four protein components in the IFT-B complexes, IFT38, IFT54, IFT57 (IFT-B2), and IFT81 (IFT-B1), contain divergent CH-like domains at their N-termini, which have been termed NN-CH domains (Schou et al. 2014). To stabilize the cilia microtubule axoneme, a supply of tubulin molecules to the interior region of the cilia is necessary. Among the NN-CH domains of the IFT components, those of IFT81 and IFT54 could bind to tubulin or tubulin dimers in vitro and only the NN-CH domain of IFT81 plays an important role in the supply of αβ-tubulin dimers to the cilia microtubule structure, working together with the N-terminal positively charged region of IFT74 (Bhogaraju et al. 2013; Kubo et al. 2016; Van De Weghe et al. 2021). On the other hand, it has been revealed that the tubulin-binding activity of the IFT54 NN-CH domain is not necessary for the supply of tubulin-molecules (Zhu et al. 2017), but is important when IFT54 functions for the regulation of cytoplasmic microtubule

dynamics. Namely, IFT54 competes with microtubule-associated protein 4 (MAP4) for binding to cytoplasmic microtubules in the cytosol and functions as a negative regulator of the stabilization of tubulin filaments (Bizet et al. 2015).

Furthermore, functions other than tubulin binding have been reported for the NN-CH domains in IFT complexes. Intriguingly, for the formation of IFT-B2 sub-complex of *Chlamydomonas reinhardtii*, the NN-CH domains of IFT38 and 57 with no tubulin-binding activity could interact with the WD40 repeat domains of IFT80 and IFT172, respectively (Lacey et al. 2023 PDBID:8BD7). This implied that the NN-CH domain could bind to protein targets other than actin/tubulin molecules. The NN-CH domain of IFT54 interacts with DYNC2I1 of the dynein-2 complex during anterograde movement, although this interaction is dispensable for ciliary dynamics (Hiyamizu et al. 2023b).

As described above, several points regarding the function of the IFT54 NN-CH domain remain obscure. Thus, structural information on the NN-CH domain of IFT54 is important for clarifying the in vivo function of the IFT54 NN-CH domain. The X-ray structure of the mouse IFT54 NN-CH domain has been elucidated, and several cryo-EM studies have been performed on the IFT machinery (Taschner et al. 2016a, b; Lacey et al. 2023; Petriman et al. 2020). In addition to such structural data, information obtained by solution NMR can be used to investigate molecular interactions.

Here, we report the ^{1}H, ^{13}C, and ^{15}N chemical shift assignments and solution structure of the divergent CH domain (NN-CH domain) of human IFT54, as determined by heteronuclear NMR methods. The structural information and assignments obtained in this study provide insights into the role of IFT54 in cytoskeletal dynamics and signaling.

Methods and experiments

Sample preparation

The DNA encoding the NN-CH domain (Met1–Lys133) of human IFT54 (UniProt accession no. Q8TDR0) was subcloned using PCR from a full-length human cDNA clone. This DNA fragment was cloned into the expression vector pCR2.1 (Invitrogen) as a fusion protein with an N-terminal native His affinity tag and tobacco etch virus (TEV) protease cleavage site. The ^{13}C/^{15}N-labeled fusion protein was synthesized using a cell-free protein expression system (Kigawa et al. 2004; Matsuda et al. 2007). The lysate was clarified by centrifugation at 16,000 ×*g* for 20 min and filtered through a 0.45-mm membrane (Merck Millipore). The clarified lysate was applied to a His-Trap column (Cytiva), eluted with a 12–500 mM imidazole gradient, and the tag was removed by incubation with TEV protease for 1 h at 30 °C. The tag-free samples were further purified by Superdex-75 gel filtration chromatography (Cytiva). For NMR measurements, the resultant samples were concentrated to approximately 1.0 mM in 20 mM d-Tris-HCl buffer (pH 7.0), containing 100 mM NaCl, 1 mM 1,4-DL-dithiothreitol-d_{10} (d-DTT), and 0.02% NaN_3 (in 90% H_2O/10% D_2O), using an Amicon Ultra-15 filter (3000 MWCO, Merck Millipore).

Consequently, the fusion protein contained an artificial tag-derived sequence (GSSGSSG) at the N-terminus derived from the expression vector. The folding state of the ^{13}C/^{15}N-labeled protein, composed of 140 residues, was checked by 2D ^{1}H–^{15}N HSQC experiments (Kigawa et al. 2004), exhibiting well-dispersed resonances (Fig. 1).

NMR spectroscopy and structure calculations

All NMR data were acquired at 298 K on Bruker 600 MHz and Bruker 800 MHz spectrometers and processed using *NMRPipe* software (Delaglio et al. 1995). Two-dimensional ^{1}H–^{13}C and ^{1}H–^{15}N HSQC spectra, three-dimensional HNCO, HN(CA)CO, HNCA, HN(CO)CA, HNCACB, CBCA(CO)NH, HBHA(CO)NH, H(CCCO)NH, (H)CC(CO)NH, HCCH-TOCSY, HCCH-COSY, CCH-TOCSY, and NOESY spectra (Cavanagh et al. 2018; Clore and Gronenborn 1998) were used to assign all carbon, nitrogen, and hydrogen atoms of the ^{13}C/^{15}N-labeled sample.

Nuclear Overhauser effect (NOE) peaks from the ^{15}N- and ^{13}C-edited 3D NOE spectroscopy (NOESY) spectra with an 80 ms mixing time were converted to distance restraints for the structure calculation of the IFT54 NN-CH domain. The three-dimensional structure of the labeled protein was determined by combining automated NOESY cross-peak assignment and structural calculations with torsion angle dynamics (Herrmann et al. 2002) implemented in the program CYANA 2.1 (Güntert et al. 1997). The dihedral angle restraints for φ and ψ were obtained from the main chain and $^{13}C^{\beta}$ chemical shift values using the TALOS program (Cornilescu et al. 1999) and by analyzing the NOESY spectra. Stereospecific assignments for the isopropyl methyl and methylene groups were determined based on the patterns of inter- and intra-residual NOE intensities (Powers et al. 1993). The structure calculation started with 200 randomized conformers using the standard CYANA-simulated annealing schedule with 40,000 torsion angle dynamics steps per conformer (Güntert and Buchner 2015). The atomic coordinates of the 20 structures with the lowest CYANA target function values were deposited in Protein Data Bank under the PDB accession code 2EQO.

Further refinements by restrained molecular dynamics simulation followed by restrained energy minimization, were performed for the 40 conformers with the lowest final

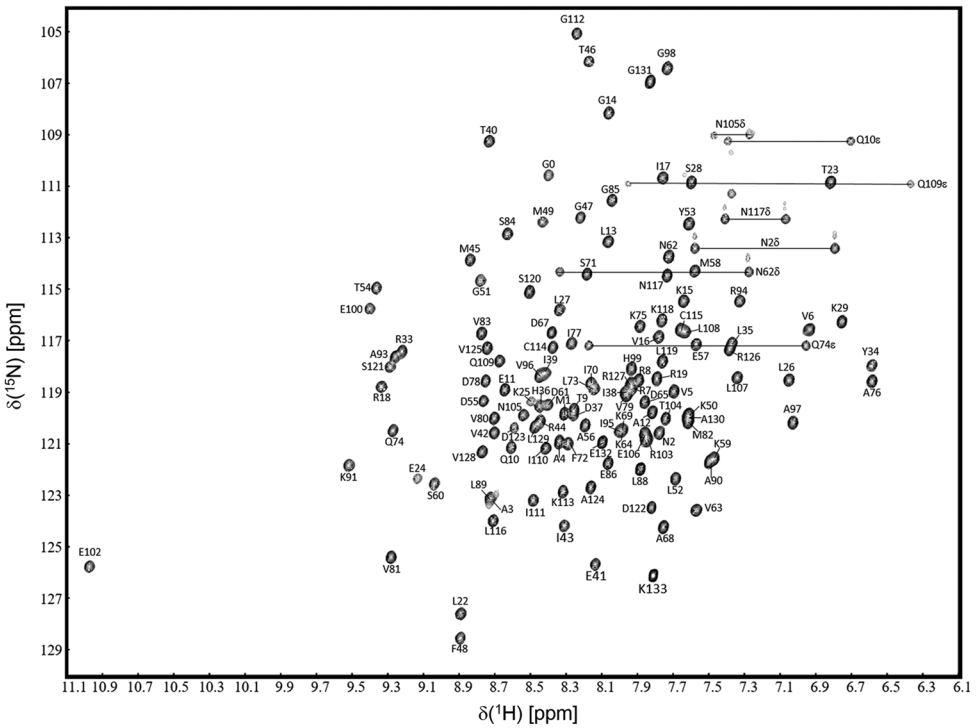

Fig. 1 Backbone resonance assignment of the NN-CH domain of human IFT54. Assigned 2D ^{1}H–^{15}N HSQC spectrum of the NN-CH domain of human IFT54. Data were acquired on a Bruker 800 MHz spectrometer by the States-TPPI method with the water-flip back pulse sequence

CYANA target function values using the Amber12 program with the Amber 2012 force field and a generalized Born model (Case et al. 2005), as described previously (Tsuda et al. 2011). Finally, 20 conformers with the lowest Amber energy values were selected as the final structures and deposited in the Protein Data Bank under the PDB accession code 8KCQ.

The PROCHECK-NMR (Laskowski et al. 1996) and MOLMOL (Koradi et al. 1996) programs were used to validate and visualize deposited structures, respectively.

Extent of assignments and data deposition

The protein used in NMR analysis was a truncated and tagged version of the human IFT54 NN-CH domain. It is comprised of 140 residues, including seven tag residues at the N-terminus. The assigned ^{1}H–^{15}N HSQC spectrum of the human IFT54 NN-CH domain is shown in Fig. 1. All backbone amide hydrogen and nitrogen atoms were assigned except for Phe39 and Lys73. In total, 100%, 100%, and 97.7% of the C^{α}, C^{β}, and C' chemical shifts were determined, respectively. Furthermore, chemical shifts of all non-exchangeable side-chain proton resonances and their related carbons, except for the H^{γ} proton of Leu59, were observed. All X-Pro peptide bonds were confirmed to be in the *trans* conformation. The chemical shift assignments for the NN-CH domain of human IFT54 were deposited in the BMRB database under accession number 36589.

Solution structure of the NN-CH domain of human IFT54

The quality of the NOESY spectra of the NN-CH domain was appropriate for straightforward structural calculations. In the ^{15}N- and ^{13}C-edited 3D NOESY spectra, 3378 non-redundant distance restraints, including 1026 long-range distance restraints, were identified. The backbone torsion angle restraints calculated using the TALOS program (Cornilescu et al. 1999) were also used for structural calculations with CYANA 2.1 (Güntert 2004; Güntert et al. 1997; Herrmann et al. 2002) and Amber12 programs (Case et al. 2005) (Supplementary Table 1). A bundle of 20 conformers representing the solution structures of the NN-CH domain of human IFT54 spanning residues 1–133 is shown in Fig. 2 (a). Five long helical structural elements (α1:3–13, α2:32–45, α3:66–84, α4:101–116, and α5:122–131) were identified. These helices are connected by the linker regions L1 (between α1 and α2), L2 (between α2 and α3), L3 (between α3 and α4), and L4 (between α4 and α5). These linker regions also contain short helical structures (h1:24–28 in L1, h2:55–58 and h2′:61–63 in L2, and h3:92–97 in L3). The main chains of the calculated structures were fitted to optimize the superposition of secondary structural elements α1, h1, α2, α3, α4, and α5. Their precision is characterized by RMSD values to the mean coordinates of 0.31 ± 0.05 Å for the backbone atoms and 1.10 ± 0.09 Å for all heavy atoms in the well-defined regions of the NN-CH domain of IFT54. For native residues 1–133, the structural quality of

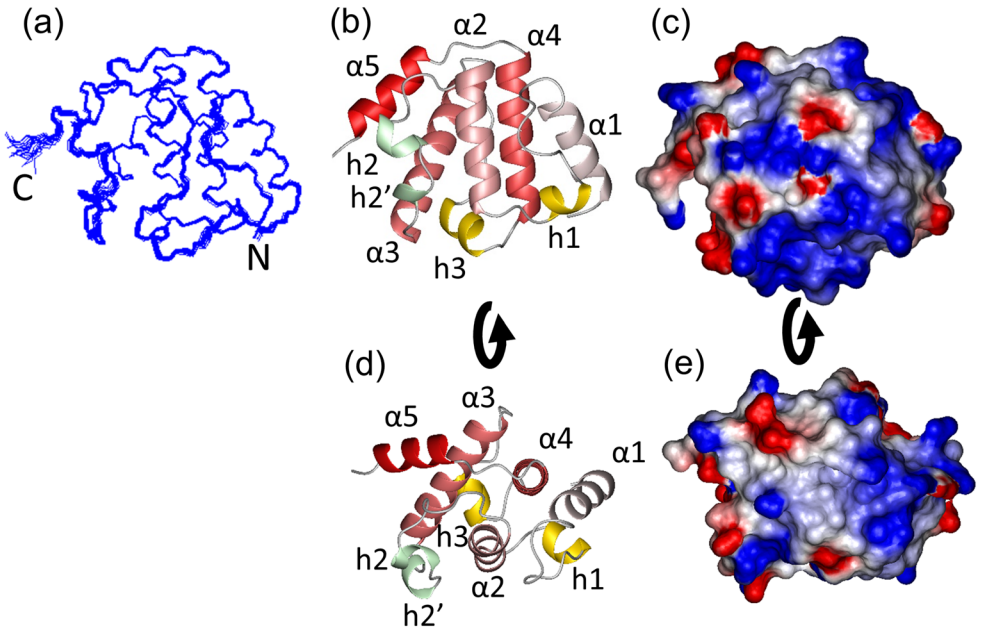

Fig. 2 Solution structures of the NN-CH domain of human IFT54. (**a**) Best-fit superposition of the backbone atoms from the 20 structures of the NN-CH domain of human IFT54 with the lowest energy, as calculated by CYANA2.1 and Amber12. (**b**) Ribbon presentation of the lowest energy structure of the IFT54 NN-CH domain. The five main helices (α1–α5) are shown in coral with increasing densities. Two short helices in loop regions (h1 in L1 and h3 in L3) are colored in gold, and two in L2 (h2 and h2') in pale green. (**c**) Electrostatic surface presentation of the IFT54 NN-CH domain in the same view as (**b**). Blue and red represent positive and negative electrostatic surface potentials, respectively. The ribbon representation (**d**) and electrostatic surface presentation (**e**) are rotated versions of (**b**) and (**c**), rotated by 90º around a horizontal axis to show a top view of (**b**) and (**c**)

the IFT54 NN-CH domain was reflected by 99.9% of the (φ, ψ) backbone torsion angle pairs in the most favored and additionally allowed regions of the Ramachandran plot, according to the PROCHECK-NMR program (Laskowski et al. 1996). Statistics regarding the quality and precision of the final 20 best conformers representing the solution structure of the IFT54 NN-CH domain are provided in Supplementary Table 1.

The present NMR solution structure of the human IFT54 NN-CH domain is almost the same as the crystallographic structure of the mouse IFT54 NN-CH domain (Taschner et al. 2016a). As described above, the canonical CH domain is thought to interact with actin and/or tubulin, and the tubulin-binding mode of the canonical CH domains has been elucidated by cryo-EM studies (Maurer et al. 2012; Zhang et al. 2015). In the case of the CH domain of EB3 (Zhang et al. 2015), the surface formed by the linker region between the α2 and α3 helices (L2 linker), the α3 helix, the linker region between the α3 and α4 helices (L3 linker), and the N-terminus of the α4 helix, intimately contacts the tubulin filaments (Supplementary Fig. 2 (a-c)). K62 and K100, which are positively charged amino-acid residues in the L2 and L3 linkers respectively, interact with negatively charged amino-acid residues of β-tubulin, and K60 in the L2 linker interacts with those of α-tubulin (identified by the Ligplot program (Laskowski et al. 2011)). In addition, K76 and K83 in the α3 helix are located near the carbonyl oxygen atoms protruding from the bottom of helical structures of α-tubulin (Supplementary Fig. 2 (a–c)). These positively charged amino-acid residues constituted a positively charged patch on the surface and played an important role in recognizing tubulin filaments (Supplementary Fig. 2 (d)). Although the NN-CH domain of IFT54 reportedly interacts with tubulin filaments, positively charged amino-acid residues are not conserved in the NN-CH domain of IFT54 at the positions corresponding to K60, K62, K83, and K100 of EB3 (Supplementary Fig. 1). Instead the positively charged patches were identified at different positions on the molecular surface of the EB3 CH domain and the IFT54 NN-CH domain (Fig. 2 (c) and (e), Supplementary Fig. 1, and Supplementary Fig. 2 (c-f)).

In addition, a comparison of the CH domain of EB3 with the NN-CH domain of IFT54 revealed structural differences in the N-terminal region preceding the α1 helix and the C-terminal region following the α4 helix. In the CH domain of EB3, the N-terminal 16 amino-acid residues, which have no canonical secondary structure, form an extended structure that surrounds the α4 helix in the free form. Interestingly, the N-terminal region extensively contacts α-tubulin in the cryo-EM structure (Supplementary Fig. 2 (a)). In contrast, the NN-CH domain of IFT54 has no corresponding N-terminal region. Furthermore, the C-terminal extension

of IFT54 contains additional α5 helix, which contacts the α3 helix and cover its surface, whereas the α5 helix of EB3 covers the surface of the α2 helix (Fig. 2 (d) and Supplementary Fig. 2 (b)). As described above, the α3 helix of the CH domain of EB3 mainly interacts with microtubule filaments. Thus, it was assumed that the NN-CH domain of IFT54 adopts a tubulin-binding mode that is different from that of the EB1 CH domain.

The NN-CH domains of IFT38 reportedly interact with the WD40 motif of IFT80 (Lacey et al. 2023). In this case, the α1 helix and the L1-linker region docked on the top of the β-barrel structure of the IFT80 WD40 motif (Supplementary Fig. 3 (a) and (b)). Some amino-acid residues in the α1 helix of IFT38 (R7 and E11) are also identified on the α1 helix of IFT54 (Arg7 and Glu11) (hereafter, amino-acid residues of IFT38 and those of IFT54 are indicated by one-letter and three-letter codes, respectively) (Supplementary Fig. 3 (b) and (c)). However, distinct structural differences have been identified between IFT38 and IFT54. First, the F3-R4 sequence at the beginning of the IFT38 NN-CH domain, which was recognized by WD40 of IFT80, was replaced with Ala3-Ala4 in the IFT54 NN-CH domain. Furthermore, in the NN-CH domain of IFT54, the position corresponding to K14 in the α1 helix of IFT38, which could interact with the acidic amino-acid residues of the WD40 domain, was occupied by a Gly residue in the IFT54 NN-CH domain. These amino-acid residues were too small to fit into the binding pocket of WD40. In addition, in the case of the IFT38 NN-CH domain, the structure of the L1 region fits well into the pocket of the WD40 motif of IFT80, as shown by the interaction of the aromatic side chain of F27 in h1 with V94 in the α4 helix and L6 in the α1 helix to sustain the extended L1 structure (Supplementary Fig. 3 (b)). In contrast, in the IFT54 NN-CH domain, a Leu residue (Leu27), which corresponds to F27 of IFT38, interacts with Thr9 and Leu13 in the C-terminal portion of the α1 helix (Supplementary Fig. 3 (c)). These interactions around Leu27 led to the formation of a non-extended structure of the L1 linker that did not fit well into the pocket of the WD40 motif of IFT80 (Supplementary Fig. 3 (d)).

Currently, some obscure points remain regarding the function of the NN-CH domain in IFT-54. Thus, we expect that this structural study will provide a basis for functional studies of the NN-CH domain of IFT54, leading to a further understanding of its function.

Supplementary Information The online version contains supplementary material available at https://doi.org/10.1007/s12104-024-10170-w.

Acknowledgements We thank Dr. Sumio Sugano of the Department of Medical Genome Sciences, Graduate School of Frontier Sciences, University of Tokyo, for providing the cDNA clone of the human IFT54 NN-CH domain.

Author contributions A. T., T. K., and M. S. prepared protein samples. K. K., W. D., M. T., K. T., F. H., T. N., N. K., and P. G. contributed to NMR experiments and structure determination. K. K. and Y. M. wrote the manuscript. Y. M. and S. Y. supervised the study.

Funding This work was supported by the RIKEN Structural Genomics/Proteomics Initiative (RSGI) and the National Project on Protein Structural and Functional Analyses of the Ministry of Education, Culture, Sports, Science and Technology of Japan. This work was also supported by *Gakuin Tokubetsu Kenkyuhi* grants from Musashino University to YM.

Data availability The chemical shift assignments for the NN-CH domain of human IFT54 were deposited in the BMRB database under accession number 36589. The atomic coordinates for the ensemble of 20 NMR structures calculated by CYANA 2.1 were deposited in the Protein Data Bank (PDB) under the accession code 2EQO and those with Amber12 refinement under accession code 8KCQ.

Declarations

Ethics approval and consent to participate Not applicable.

Consent for publication Not applicable.

Competing interests The authors declare no competing interests.

References

Berbari NF, Kin NW, Sharma N, Michaud EJ, Kesterson RA, Yoder BK (2011) Mutations in Traf3ip1 reveal defects in ciliogenesis, embryonic development, and altered cell size regulation. Dev Biol 360:66–76. https://doi.org/10.1016/j.ydbio.2011.09.001

Bhogaraju S, Cajanek L, Fort C, Blisnick T, Weber K, Taschner M, Mizuno N, Lamla S, Bastin P, Nigg EA, Lorentzen E (2013) Molecular basis of tubulin transport within the cilium by IFT74 and IFT81. Science 341:1009–1012. https://doi.org/10.1126/science.1240985

Bizet AA, Becker-Heck A, Ryan R, Weber K, Filhol E, Krug P, Halbritter J, Delous M, Lasbennes MC, Linghu B, Oakeley EJ, Zarhrate M, Nitschké P, Garfa-Traore M, Serluca F, Yang F, Bouwmeester T, Pinson L, Cassuto E, Dubot P, Elshakhs NAS, Sahel JA, Salomon R, Drummond IA, Gubler MC, Antignac C, Chibout S, Szustakowski JD, Hildebrandt F, Lorentzen E, Sailer AW, Benmerah A, Saint-Mezard P, Saunier S (2015) Mutations in TRAF3IP1/IFT54 reveal a new role for IFT proteins in microtubule stabilization. Nat Commun 6:8666. https://doi.org/10.1038/ncomms9666

Braun DA, Hildebrandt F (2017) Ciliopathies. Cold Spring Harb Perspect Biol 9:a028191. https://doi.org/10.1101/cshperspect.a028191

Case DA, Cheatham TE, Darden T, Gohlke H, Luo R, Merz KM Jr., Onufriev A, Simmerling C, Wang B, Woods RJ (2005) The Amber biomolecular simulation programs. J Comput Chem 26:1668–1688. https://doi.org/10.1002/jcc.20290

Cavanagh J, Fairbrother WJ, Palmer AG III, Skelton NJ (2018) Protein NMR spectroscopy: principles and practice. Academic, San Diego

Clore GM, Gronenborn AM (1998) New methods of structure refinement for macromolecular structure determination by NMR. Proc Natl Acad Sci U S A 95:5891–5898. https://doi.org/10.1073/pnas.95.11.5891

Cole DG, Diener DR, Himelblau AL, Beech PL, Fuster JC, Rosenbaum JL (1998) Chlamydomonas kinesin-II–dependent Intraflagellar transport (IFT): IFT particles contain proteins required for ciliary assembly in Caenorhabditis elegans sensory neurons. J Cell Biol 141:993–1008. https://doi.org/10.1083/jcb.141.4.993

Cornilescu G, Delaglio F, Bax A (1999) Protein backbone angle restraints from searching a database for chemical shift and sequence homology. J Biomol NMR 13:289–302. https://doi.org/10.1023/a:1008392405740

Delaglio F, Grzesiek S, Vuister GW, Zhu G, Pfeifer J, Bax A (1995) NMRPipe: a multidimensional spectral processing system based on UNIX pipes. J Biomol NMR 6:277–293. https://doi.org/10.1007/BF00197809

Funabashi T, Katoh Y, Okazaki M, Sugawa M, Nakayama K (2018) Interaction of heterotrimeric kinesin-II with IFT-B-connecting tetramer is crucial for ciliogenesis. J Cell Biol 217:2867–2876. https://doi.org/10.1083/jcb.201801039

Güntert P (2004) Automated NMR structure calculation with CYANA. Methods Mol Biol 278:353–378. https://doi.org/10.1385/1-59259-809-9:353

Güntert P, Buchner L (2015) Combined automated NOE assignment and structure calculation with CYANA. J Biomol NMR 62:453–471. https://doi.org/10.1007/s10858-015-9924-9

Güntert P, Mumenthaler C, Wüthrich K (1997) Torsion angle dynamics for NMR structure calculation with the new program DYANA. J Mol Biol 273:283–298. https://doi.org/10.1006/jmbi.1997.1284

Herrmann T, Güntert P, Wüthrich K (2002) Protein NMR structure determination with automated NOE assignment using the new software CANDID and the torsion angle dynamics algorithm DYANA. J Mol Biol 319:209–227. https://doi.org/10.1016/s0022-2836(02)00241-3

Hiyamizu S, Qiu H, Tsurumi Y, Hamada Y, Katoh Y, Nakayama K (2023a) Dynein-2-driven intraciliary retrograde trafficking indirectly requires multiple interactions of IFT54 in the IFT-B complex with the dynein-2 complex. Biol Open 12:bio059976. https://doi.org/10.1242/bio.059976

Hiyamizu S, Qiu H, Vuolo L, Stevenson NL, Shak C, Heesom KJ, Hamada Y, Tsurumi Y, Chiba S, Katoh Y, Stephens DJ, Nakayama K (2023b) Multiple interactions of the dynein-2 complex with the IFT-B complex are required for effective intraflagellar transport. J Cell Sci 136:jcs260462. https://doi.org/10.1242/jcs.260462

Huangfu D, Liu A, Rakeman AS, Murcia NS, Niswander L, Anderson KV (2003) Hedgehog signalling in the mouse requires intraflagellar transport proteins. Nature 2003, 426:83–87. https://doi.org/10.1038/nature02061

Ishikawa H, Marshall WF (2011) Ciliogenesis: building the cell's antenna. Nat Rev Mol Cell Biol 12:222–234. https://doi.org/10.1038/nrm3085

Ishikawa H, Marshall WF (2017) Intraflagellar transport and ciliary dynamics. Cold Spring Harb Perspect Biol 9:a021998. https://doi.org/10.1101/cshperspect.a021998

Jordan MA, Diener DR, Stepanek L, Pigino G (2018) The cryo-EM structure of intraflagellar transport trains reveals how dynein is inactivated to ensure unidirectional anterograde movement in cilia. Nat Cell Biol 20:1250–1255. https://doi.org/10.1038/s41556-018-0213-1

Katoh Y, Terada M, Nishijima Y, Takei R, Nozaki S, Hamada H, Nakayama K (2016) Overall Architecture of the Intraflagellar Transport (IFT)-B complex containing Cluap1/IFT38 as an essential component of the IFT-B Peripheral Subcomplex. J Biol Chem 291:10962–10975. https://doi.org/10.1074/jbc.M116.713883

Kigawa T, Yabuki T, Matsuda N, Matsuda T, Nakajima R, Tanaka A, Yokoyama S (2004) Preparation of Escherichia coli cell extract for highly productive cell-free protein expression. J Struct Funct Genomics 5:63–68. https://doi.org/10.1023/B:JSFG.0000029204.57846.7d

Klena N, Pigino G (2022) Structural biology of cilia and intraflagellar transport. Annu Rev Cell Dev Biol 38:103–123. https://doi.org/10.1146/annurev-cellbio-120219-034238

Koradi R, Billeter M, Wüthrich K (1996) MOLMOL: a program for display and analysis of macromolecular structures. J Mol Graph 14:51–55. https://doi.org/10.1016/0263-7855(96)00009-4

Kozminski KG, Beech PL, Rosenbaum JL (1995) The Chlamydomonas kinesinlike protein FLA10 is involved in motility associated with the flagellar membrane. J Cell Biol 131:1517–1527. https://doi.org/10.1083/jcb.131.6.1517

Kubo T, Brown JM, Bellve K, Craige B, Craft JM, Fogarty K, Lechtreck KF, Witman GB (2016) Together, the IFT81 and IFT74 N-termini form the main module for intraflagellar transport of tubulin. J Cell Sci 129:2106–2119. https://doi.org/10.1242/jcs.187120

Lacey SE, Foster HE, Pigino G (2023) The molecular structure of IFT-A and IFT-B in anterograde intraflagellar transport trains. Nat Struct Mol Biol 30:584–593. https://doi.org/10.1038/s41594-022-00905-5

Laskowski RA, Swindells MB (2011) LigPlot+: multiple ligand-protein interaction diagrams for drug discovery. J Chem Inf Model 51:2778–2786. https://doi.org/10.1021/ci200227u

Laskowski RA, Rullmannn JA, MacArthur MW, Kaptein R, Thornton JM (1996) AQUA and PROCHECK-NMR: programs for checking the quality of protein structures solved by NMR. J Biomol NMR 8:477–486. https://doi.org/10.1007/BF00228148

Ling L, Goeddel DV (2000) MIP-T3, a novel protein linking tumor necrosis factor receptor-associated factor 3 to the microtubule network. J Biol Chem 275:23852–23860. https://doi.org/10.1074/jbc.M001095200

Matsuda T, Koshiba S, Tochio N, Seki E, Iwasaki N, Yabuki T, Inoue M, Yokoyama S, Kigawa T (2007) Improving cell-free protein synthesis for stable-isotope labeling. J Biomol NMR 37:225–229. https://doi.org/10.1007/s10858-006-9127-5

Maurer SP, Fourniol FJ, Bohner G, Moores CA, Surrey T (2012) EBs recognize a nucleotide-dependent structural cap at growing microtubule ends. Cell. https://doi.org/10.1016/j.cell.2012.02.049. 149:371 – 82

Nachury MV, Loktev AV, Zhang Q, Westlake CJ, Peränen J, Merdes A, Slusarski DC, Scheller RH, Bazan JF, Sheffield VC, Jackson PK (2007) A core complex of BBS proteins cooperates with the GTPase Rab8 to promote ciliary membrane biogenesis. Cell 129:1201–1213. https://doi.org/10.1016/j.cell.2007.03.053

Petriman NA, Lorentzen E (2020) Structural insights into the architecture and assembly of eukaryotic flagella. Microb Cell. 2020 7:289–299. https://doi.org/10.15698/mic2020.11.734

Petriman NA, Loureiro-López M, Taschner M, Zacharia NK, Georgieva MM, Boegholm N, Wang J, Mourão A, Russell RB, Andersen JS, Lorentzen E (2022) Biochemically validated structural model of the 15-subunit intraflagellar transport complex IFT-B. EMBO J 41:e112440. https://doi.org/10.15252/embj.2022112440

Piperno G, Siuda E, Henderson S, Segil M, Vaananen H, Sassaroli M (1998) Distinct mutants of retrograde intraflagellar transport (IFT) share similar morphological and molecular defects. J Cell Biol 143:1591–1601. https://doi.org/10.1083/jcb.143.6.1591

Powers R, Garrett DS, March CJ, Frieden EA, Gronenborn AM, Clore GM (1993) The high-resolution, three-dimensional solution structure of human interleukin-4 determined by multidimensional heteronuclear magnetic resonance spectroscopy. Biochemistry 32:6744–6762. https://doi.org/10.1021/bi00077a030

Richey EA, Qin H (2012) Dissecting the sequential assembly and localization of intraflagellar transport particle complex B in Chlamydomonas. PLoS ONE 7e43118. https://doi.org/10.1371/journal.pone.0043118

Rosenbaum JL, Witman GB (2002) Intraflagellar transport. Nat Rev Mol Cell Biol 3:813–825. https://doi.org/10.1038/nrm952

Salomon R, Saunier S, Niaudet P (2009) Nephronophthisis. Pediatr. Nephrol. 24:2333–2344 (2009) https://doi.org/10.1007/s00467-008-0840-z

Schou KB, Andersen JS, Pedersen LB (2014) A divergent calponin homology (NN-CH) domain defines a novel family: implications for evolution of ciliary IFT complex B proteins. Bioinformatics 30:899–902. https://doi.org/10.1093/bioinformatics/btt661

Taschner M, Lorentzen E (2016a) The intraflagellar transport machinery. Cold Spring Harb Perspect Biol 8:a028092. https://doi.org/10.1101/cshperspect.a028092

Taschner M, Weber K, Mourão A, Vetter M, Awasthi M, Stiegler M, Bhogaraju S, Lorentzen E (2016b) Intraflagellar transport proteins 172, 80, 57, 54, 38, and 20 form a stable tubulin-binding IFT-B2 complex. EMBO J 35:773–790. https://doi.org/10.15252/embj.201593164

Tobin JL, Beales PL (2009) The nonmotile ciliopathies. Genet Med 11:386–402. https://doi.org/10.1097/GIM.0b013e3181a02882

Tsuda K, Someya T, Kuwasako K, Takahashi M, He F, Unzai S, Inoue M, Harada T, Watanabe S, Terada T, Kobayashi N, Shirouzu M, Kigawa T, Tanaka A, Sugano S, Guntert P, Yokoyama S, Muto Y (2011) Structural basis for the dual RNA-recognition modes of human Tra2-β RRM. Nucleic Acids Res 39:1538–1553. https://doi.org/10.1093/nar/gkq854

Van De Weghe JC, Giordano JL, Mathijssen IB, Mojarrad M, Lugtenberg D, Miller CV, Dempsey JC, Mohajeri MSA, van Leeuwen E, Pajkrt E, Klaver CCW, Houlden H, Eslahi A, Waters AM, University of Washington Center for Mendelian Genomics, Bamshad MJ, Nickerson DA, Aggarwal VS, de Vries BBA, Maroofian R, Doherty D (2021) TMEM218 dysfunction causes ciliopathies, including Joubert and Meckel syndromes. HGG Adv 2:100016. https://doi.org/10.1016/j.xhgg.2020.100016

Wheway G, Nazlamova L, Hancock JT (2018) Signaling through the primary cilium. Front Cell Dev Biol 6:1–13. https://doi.org/10.3389/fcell.2018.00008

Wingfield JL, Mengoni I, Bomberger H, Jiang Y-Y, Walsh JD, Brown JM, Picariello T, Cochran DA, Zhu B, Pan J et al (2017) IFT trains in different stages of assembly queue at the ciliary base for consecutive release into the cilium. Elife 6:e26609. https://doi.org/10.7554/eLife.26609

Wolf MTF (2015) Nephronophthisis and related syndromes. Curr Opin Pediatr 27:201–211. https://doi.org/10.1097/MOP.0000000000000194

Yin LM, Schnoor M, Jun CD (2020) Structural characteristics, Binding Partners and related diseases of the Calponin homology (CH) domain. Front Cell Dev Biol 8:342. https://doi.org/10.3389/fcell.2020.00342

Zhang R, Alushin GM, Brown A, Nogales E (2015) Mechanistic origin of Microtubule dynamic instability and its modulation by EB proteins. Cell 162:849–859. https://doi.org/10.1016/j.cell.2015.07.012

Zhu X, Liang Y, Gao F, Pan J (2017) IFT54 regulates IFT20 stability but is not essential for tubulin transport during ciliogenesis. Cell Mol Life Sci 74:3425–3437. https://doi.org/10.1007/s00018-017-2525-x

Zhu X, Wang J, Li S, Lechtreck K, Pan J (2021) IFT54 directly interacts with kinesin-II and IFT dynein to regulate anterograde intraflagellar transport. EMBO J 40:e105781. https://doi.org/10.15252/embj.2020105781